ISSN 0915-633X

NATIONAL INSTITUTE FOR FUSION SCIENCE

Late States of Incompressible 2D Decaying Vorticity Fields

E. Segre and S. Kida

(Received - July 24, 1997)

NIFS-503 Aug. 1997

RESEARCH REPORT
NIFS Series

NAGOYA, JAPAN

Late states of incompressible 2D decaying vorticity fields

Enrico Segre [1]

Dipartimento di Ingegneria Aeronautica e Spaziale, Politecnico di Torino, Italy

and

Shigeo Kida

Theory and Computer Simulation Center, National Institute for Fusion Science, Toki 509-52, Japan

Two-dimensional decaying turbulent flow is known to approach apparently stable states after a long time evolution. A few theories and models have been so far proposed to account for this relaxation. In this paper, we compare results of numerical experiments with the predictions of these theories to assess their applicability. We study the long time decay of initially multilevel vorticity fields on the periodic box, and characterize the outcoming final states. Our final states do not match the predictions of the theories; a broader variety of dipole profiles, as well as nonstationary final states are found. The problem of the robustness of the relaxational state with respect to variations of the Reynolds number and different numerical resolution is addressed. The observed configurations also do not necessarily possess the maximal energy, in contrast to what is anticipated by some of the theories. We are led to conclude that the mixing of the vorticity is generally not ergodic, and that some metastable configurations may inhibit the attainment of an equilibrium state.

Key words: Two-dimensional Turbulence, Vorticity, Statistical Theories.
PACS codes: 47.27.Gs, 47.32.-y, 05.45.+b

[1] Correspondence to Dr. Enrico Segre, Dipartimento di Ingegneria Aeronautica e Spaziale, Politecnico, corso Duca degli Abruzzi 24, I-10129 Torino, Italy, tel. +39-11-564-6853, fax +39-11-564-6853, email `segre@polito.it`

1 Introduction and motivations

The decay of the vorticity field of a two-dimensional incompressible fluid, which obeys to the unforced Navier-Stokes equation, shows several interesting features. Stable large scale structures may form, organize themselves on the scale of the accessible domain, and survive for a long time before being ultimately damped by the dissipation. Occurrences of such structures are observed in numerical and laboratory experiments, as well as in planetary scale flows. We will call from here on such configurations "final"; by that we mean subjected only to viscous decay and no more to filamentation and mixing. Provided that the Reynolds number of the flow is large enough, the timescales for these two processes can be very different. We are concerned with the appearance of final states emerging from arbitrary initial conditions, with their robustness and their predictability. Most of the numerical simulations presented in the literature start from random initial conditions, whose Fourier spectra decay variously in k, with uncorrelated phases. In such cases, intermediate states with few isolated vortex cores are observed. In the traditional scenario [2], the progressive merging of likely signed vortex cores is then observed. Several papers in the literature deal with the merging process, either analyzing the evolution in time of the vortex census, or modelling the process with simplified dynamics. Less attention has been so far devoted to the actual characteristics of the latest state of the field.

A few explanations for the occurrence of final states have been proposed so far. We will refer specifically to those theories, which are formulated in the physical space rather than in the Fourier one: the minimum enstrophy assumption and the maximal entropy state statistical theory [35,44]. Some numerical evidence has also been invoked to reconnect computed results with the Joyce-Montgomery equation, which is originally derived for the mean field limit of a system of point vortices [37].

We consider several cases of decay of vorticity fields. All cases start from initial conditions which should be generic and appropriate for the application of the final state theories. Our results contrast with the conclusion that an universal state emerges out of the relaxation, without memory of the dynamical path which led to it. In fact, we even see that the final 'state' may be unsteady: some fields attain a late time configuration which is not stationary. Such late fields may move quasiperiodically and steadily, being just slowly damped by the (arbitrary small) dissipation.

This paper is organized as follows: in section 2 we briefly review the treatment of the problem of two-dimensional turbulent decay, highlighting the different variational problems which are solved to find the final state, and the functional relations $\omega(\psi)$ derived. In section 3 we describe the numerical experiments per-

formed. Finally, in section 4 we comment on the open aspects which require further investigation. A number of remarks which are related to the maximization of the energy and its relevance for the final state are left for the Appendix.

2 Review of the available theories

Let us first recall the notation. As is well known, the equation of motion for the vorticity $\omega(\mathbf{x})$ is written as

$$\omega_t(\mathbf{x}) = -\mathbf{v}(\mathbf{x}) \cdot \nabla\omega(\mathbf{x}) + \nu\nabla^2\omega(\mathbf{x}) = J(\omega(\mathbf{x}), \psi(\mathbf{x})) + \nu\nabla^2\omega(\mathbf{x}) \,. \quad (1)$$

In (1), ψ denotes the streamfunction, obtained from $\omega(\mathbf{x})$ by means of the Green function G of the Laplacian operator

$$\psi(\mathbf{x}) = \int G(\mathbf{x}', \mathbf{x})\omega(\mathbf{x}')d^2\mathbf{x} \,. \quad (2)$$

The integral is carried on the fluid domain with the proper boundary conditions, so that $\nabla^2\psi = -\omega$. Introducing the notation $\nabla^\perp = (\partial_y, -\partial_x)$, we may write $\nabla^\perp\psi = \mathbf{v}$ and $J(\omega, \psi) = \nabla\omega \cdot \nabla^\perp\psi$. The energy of the field is defined as

$$E = \frac{1}{2}\int \psi(\mathbf{x})\omega(\mathbf{x})d^2\mathbf{x} \,, \quad (3)$$

and the moments of the vorticity as

$$Q_l = \frac{1}{2}\int \omega^l(\mathbf{x})d^2\mathbf{x} \,, \quad (4)$$

with l a positive integer. The quantity $Q_2(\equiv Q)$ is traditionally called the enstrophy. Another global quantity which is defined is the palinstrophy

$$P = \frac{1}{2}\int [\nabla\omega(\mathbf{x})]^2 \, d^2\mathbf{x} \,. \quad (5)$$

These quantities evolve in time according to:

$$\begin{aligned} E_t &= \quad -2\nu Q \,, \qquad Q_t = -2\nu P \,, \\ Q_{l,t} &= -l(l-1)\nu \int \omega(\mathbf{x})^{l-2} \, [\nabla\omega(\mathbf{x})]^2 \, d^2\mathbf{x} \,. \end{aligned} \quad (6)$$

E and all Q_l are constants of motion if $\nu = 0$. In the limit of vanishing viscosity, E is a constant of motion, but Q may not be, because P can get larger inversely proportional to ν.

We refer to theories which predict the final state as the most probable outcome of the decay. In a way or the other, all these models assume a distinction between the fully detailed dynamics expressed by equation (1), and that of a reduced set of macroscopically observable quantities. The evolution of the field is seen as a process in which the initial information is lost in some way. As a deliberate simplification, the final state is sought as the one which is fully described only by a few macroscopical constraints, which are often called "rugged invariants". Such theories treat the viscous, finite resolution problem, as one in which some quantities are "better" conserved than the rest, in place of the infinite set of the inviscid case. There is indeed some ambiguity, and properly speaking the case $\nu = 0$ is different from the limit $\nu \to 0$, since in the former infinitely steep gradients might form. Where possible, methods of statistical mechanics are applied, and some extremum principle is invoked. A comprehensive review of the various positions can be found elsewhere (e.g. [35]); here we recall them briefly, and discuss their conclusions.

2.1 Equilibrium Fourier spectra

A first group of theories is formulated in the Fourier space. The older Kraichnan–Batchelor–Leith statistical theory [27] predicts a Fourier spectrum $E(k) \sim k^{-3}$, relying on the assumption of the locality of the interactions among the components. An improvement by [28], based on the test-field-model closure approximation, corrected this spectrum to $E(k) \sim k^{-3} (\ln k/k_0)^{\frac{1}{3}}$. While some numerical simulations [26,3] support these spectra, quite different spectra have been observed by others (see for example [33]) The reason of the discrepancy is not clear, though the formation of stable structures may take a key role.

A later theory due to Kraichnan [29,7] proposes a statistical mechanics for the energies of the Fourier components. An ultaviolet cutoff in k has to be enforced. Only E and Q are assumed to be constants of motion, and are fixed as constraints. No correlation is assumed between the phases of $\omega(k)$, and no other moment of the vorticity is conserved. This theory predicts a statistical equilibrium spectrum

$$E(k) = \frac{1}{\beta k^2 + \alpha}, \qquad Q(k) = \frac{k^2}{\beta k^2 + \alpha}, \tag{7}$$

with arbitrary constants α and β. The agreement of these spectra with those coming from numerical simulations, and expecially with ours, is controversial.

2.2 Point vortex systems

A second line of reasoning considers the statistical properties of an ensemble of point vortices. The rationale for connecting vorticity fields with such systems is that a system of point vortices approximates weakly, in the continuum limit, the Euler equation [5,16,6]; the full Navier-Stokes equation can be emulated by point vortices which diffuse with an additional Brownian motion [15]. An entropy of the system is introduced and maximized. In the mean field limit, a differential equation is derived for the equilibrium configuration [36,24,41]:

$$\omega_0(\mathbf{x}) = -\nabla^2\psi_0(\mathbf{x}) = c_1\, e^{-\beta\psi_0(\mathbf{x})} - c_2\, e^{\beta\psi_0(\mathbf{x})}\ . \tag{8}$$

This provides us with a first example of an equation which relates functionally ω_0 and ψ_0. As is known, the functional dependence implies the stationarity of the motion, in the case of null dissipation. In the special case of an equal number of opposite charged positive and negative vortices, the Joyce-Montgomery equation reduces to the sinh-Poisson equation

$$\omega_0(\mathbf{x}) = \lambda^2 \sinh(|\beta|\psi_0(\mathbf{x}))\,. \tag{9}$$

This equation has been furthermore studied referring to the inverse scattering theory for the sin-Gordon equation [49]. Solutions possessing simple scattering spectra can be constructed, but no dynamical analysis, beyond a comparison of shapes, was done.

Montgomery, Shan and Matthaeus [37] give an interpretation of the problem which is somehow related. They propose a decomposition of the vorticity field in four non-physical positive subfields. An entropy of the form

$$S = \int \omega_i \ln \omega_i d^2\mathbf{x} \tag{10}$$

is then maximized individually for each subfield, with the proper constraints on the total energy and vorticity. The remaining arbitrary constants are fitted to the results of a single high resolution, high Reynolds number Navier–Stokes numerical simulation. For that case, they achieve a good fit of the $\psi(\omega)$ scatterplot at late times. For our purposes, it suffices to note that their final relation implies

$$\omega_0(\mathbf{x}) = c_1\, e^{-\beta\psi_0(\mathbf{x})} - c_2\, e^{\beta\psi_0(\mathbf{x})} + c_3\,, \tag{11}$$

which is an elaboration of (8), and can be assimilated to equation (21) in the case of 3 levels.

2.3 Minimum enstrophy principle

The identification of the final state as the one with lowest enstrophy dates back to Bretherton and Haidvogel [4]. They argued that while the energy can almost be conserved by a good numerical scheme, the vorticity filamentates progressively and smoothes out. Arguments related to the universality of the energy-enstrophy cascades, as in the Kraichnan–Batchelor–Leith theory, would predict for instance a behavior of $Q(t) \sim t^{-2}$ [9,1]. The idea of a faster decay of the enstrophy with respect to the energy is often referred to as the "selective decay hypothesis". The final state is consequently found variationally, by minimizing Q with constrained E. According to this hypothesis, axisymmetric vortex shapes on the infinite plane can be calculated [30]. Time asymptotic estimates for closed square box solutions are discussed by Van Groesen [51].

In the case of doubly periodical boundary conditions, it is straightforward to find a solution. Imposing

$$\frac{\delta}{\delta\omega}\frac{1}{2}\int(\omega^2 - \lambda\psi\omega)d^2\mathbf{x} = 0\,, \tag{12}$$

we obtain

$$\omega_0(\psi_0) = \lambda\psi_0\,, \tag{13}$$

which on the periodic square admits solutions of the form $\omega_0(\mathbf{x}) = \sum\omega_\mathbf{k}\,\mathrm{e}^{\mathrm{i}\mathbf{k}\cdot\mathbf{x}}$, with $|\mathbf{k}|^2 = \lambda$ equal to a squared integer. This implies that $Q = \lambda E$. For a given energy the minimal enstrophy is then achieved for $\lambda = 1$, and the general solution becomes $\omega_0(\mathbf{x}) = \omega_1\cos(x + a) + \omega_2\cos(y + b)$, with ω_1, ω_2, a and b being arbitrary constants. Linear combinations of such sinusoidal solutions with different k (i.e. complete Fourier series) do *not* satisfy the requirement. In the numerical experiments we find final states of completely different forms. We remark however that this principle was introduced for flows with additional "topographic" terms in (1), and we do not exclude that it may provide realistic results in cases where these are dominant.

2.4 Vortex censuses and punctuated dynamics

In a number of papers, appeared around 1990, the late lowering of the enstrophy is solely explained as a result of progressive vortex mergings [34,31,9]. These papers consider situations with an intermediate time dynamics dominated by many well separated vortex cores, which behave approximately like

point vortices. The subsequent evolution is schematized by a progressive collapse and merging of these objects. Statistics of the number N of cores in time, models for the probability of merging are examined, and eventually lead to different scalings of $Q(t)$. The final state is assumed to be a dipole, and its properties are sought by scaling the relevant quantities down to $N = 2$. A popular model is the punctuated Hamiltonian system [8], which is the traditional point vortex model fitted with a nonconservative merging as vortices get close enough. Such models can be further elaborated accounting for extended cores [43].

2.5 Maximum entropy theory

The reasoning is based on the combinatorics of infinitesimal vorticity patches, at a scale smaller than that which determines the energy of the configuration. We follow the notation of Miller, Weichman and Cross [35], rather than the equivalent one of Robert and Sommeria [44]. The theory is indeed intended only for the Euler equation; Weichman [53] proposes an additional argument in order to include the viscosity in connection with the underresolution, which seems incorrect. The theory mimics the statistical mechanics of a many particle system. A given distribution of (infinitesimally grained) vorticity is assimilated to a microstate; at the macroscopical level, only a coarse averaged vorticity $\overline{\omega}(\mathbf{x})$ can be observed. The fine scale structure is remembered by introducing a local probability distribution $n(\mathbf{x}, \sigma)d\sigma$ of vorticity, which says how large is the probability of having a microscale vorticity $\sigma \leq \omega(\mathbf{x}) < \sigma + d\sigma$ at point $\mathbf{x}$. The macroscopic averaged vorticity is then

$$\overline{\omega}(\mathbf{x}) = \int \sigma n(\mathbf{x}, \sigma) d\sigma. \tag{14}$$

The macrostate is the field of probability over the whole domain. Any microscale distribution of vorticity, which looks on the macroscale like that probability, is said to be a compatible microstate. The fluid is expected to relax to the macrostate which can be achieved in the largest number of ways, and thus is maximally probable. The theory relies on the strong assumption, that the microscale mixing of vorticity is ergodic. This means that the available vorticity is completely free to mix in any possible (area preserving) way, so that only the probability determines which outcome is likely to be observed. A macrocanonical approach is undertaken. A free energy

$$F(\{n\}) = -S(\{n\}) - \beta E(\{n\}) + \sum_{l=0}^{\infty} \mu_l Q_l. \tag{15}$$

is maximized. Here $S(\{n\})$ is the entropy function

$$S(\{n\}) = -\int n(\mathbf{x},\sigma)\ln n(\mathbf{x},\sigma)d^2\mathbf{x}d\sigma\,, \tag{16}$$

the energy, expressed in terms of $n(\mathbf{x},\sigma)$, is

$$E(\{n\}) = \frac{1}{2}\int \sigma\sigma' n(\mathbf{x},\sigma)n(\mathbf{x}',\sigma')G(\mathbf{x}',\mathbf{x})d^2\mathbf{x}d^2\mathbf{x}'d\sigma d\sigma'\,, \tag{17}$$

and the constants of motion are multiplied by appropriate Lagrange factors and added to $F(\{n\})$.

The constraints to be imposed are E = constant, $\int n d\sigma = 1$ and $\int n d^2\mathbf{x} = g(\sigma)$. The function $g(\sigma)$ is the global vorticity distribution, which should be invariant for microscale inviscid flows. To implement the last constraint, the conservation of all moments of the vorticity is instead required. It is assumed to be sufficient that the infinite set of moments of the vorticity are conserved without requiring the topological correctness of the flux. In other words, it is assumed that the area preserving vorticity mappings are dense (at least in the coarse average) in the topologically feasible fluxes. Using $g(\sigma)$ instead of Q_l,

$$\sum_{l=0}^{\infty}\mu_l\int\overline{\omega}^l d^2\mathbf{x} = \sum_{l=0}^{\infty}\mu_l\int\sigma^l g(\sigma)d\sigma = \int\mu(\sigma)n(\mathbf{x},\sigma)d\sigma d^2\mathbf{x}\,. \tag{18}$$

Functional derivation with respect to $n(\mathbf{x},\sigma)$ and algebraic manipulation lead to the system

$$\begin{aligned} n_0(\mathbf{x},\sigma) &= \frac{e^{-\beta(\sigma\psi_0(\mathbf{x})-\mu(\sigma))}}{\int e^{-\beta(\sigma\psi_0(\mathbf{x})-\mu(\sigma))}\,d\sigma}, \\ \omega_0(\mathbf{x}) &= \int\sigma n_0(\mathbf{x},\sigma)d\sigma = -\nabla^2\psi_0(\mathbf{x})\,, \end{aligned} \tag{19}$$

which has to be solved in order to find the maximally probable macrostate $n_0(\mathbf{x},\sigma)$. In this procedure, the dependencies of β on E and of $\mu(\sigma)$ on $g(\sigma)$ are left as implicit; their actual form is supposed to be found only after solving consistently the system. It is also assumed, but not proven, that Lagrange multipliers can be determined for any physically accessible values of the conserved quantities. The system (19) does not in fact say very much. For $\beta < 0$, it states that the probability of having at $\mathbf{x}$ a vorticity of the same sign of $\psi_0(\mathbf{x})$ grows with σ, but is shaped by the weight factor $\exp[\beta\mu(\sigma)]$. For $\beta > 0$, the same applies to a vorticity opposite in sign to $\psi_0(\mathbf{x})$. The fact that $\beta < 0$ in physical situations is inferred in comparison with the case of a 2D Coulomb gas [35].

Robert and Sommeria [45] also derive an evolution equation for the approach to the maximum entropy state in this framework. Going further on, Jüttner, Thess and Turkington [23] propose a way to include random forcing in the maximum entropy theory.

Particular forms of $\psi_0(\omega_0)$ can be found only with additional hypotheses. If, for instance, the vorticity takes only N different values $(\omega_1, \ldots, \omega_N)$, then $n(\mathbf{x}, \sigma)$ will be everywhere a sum of delta functions. The system (19) becomes

$$n_0(\mathbf{x}, \sigma) = \frac{\sum_{i=1}^{N} \mathrm{e}^{-\beta[\omega_i \psi_0(\mathbf{x}) - \mu(\omega_i)]}\, \delta(\sigma - \omega_i)}{\sum_{i=1}^{N} \mathrm{e}^{-\beta[\omega_i \psi_0(\mathbf{x}) - \mu(\omega_i)]}} = \sum_{i=1}^{N} n_i(\mathbf{x}) \delta(\sigma - \omega_i)\,, \tag{20}$$

$$\omega_0(\mathbf{x}) = \frac{\sum_{i=1}^{N} \omega_i\, \mathrm{e}^{-\beta \omega_i \psi_0(\mathbf{x})}\, \mathrm{e}^{\beta \mu(\omega_i)}}{\sum_{i=1}^{N} \mathrm{e}^{-\beta[\omega_i \psi_0(\mathbf{x}) - \mu(\omega_i)]}} = \sum_{i=1}^{N} n_i(\mathbf{x}) \omega_i\,. \tag{21}$$

The latter equation expresses a single valued relation $\omega_0(\psi_0)$. Inverted as $\psi_0(\omega_0)$, it may eventually be multiple-branched. Specifically, for two opposite levels $\omega_1 = -\omega_2$, (21) becomes

$$\omega_0(\mathbf{x}) = \tanh\left(-\beta \omega_1 \psi_0(\mathbf{x}) + \beta \frac{\mu(\omega_1) - \mu(-\omega_1)}{2}\right)\,. \tag{22}$$

The slope of the curve in the (ω, ψ) plane is determined by β, which depends on the energy; the position of the origin is fixed by $\mu(\omega_1) - \mu(-\omega_1)$, which in turn can be expressed as a function of Q (all the higher moments of the vorticity are related to Q by the limitation to two levels).

For a two-level vorticity distribution it is even possible to reconstruct $n(\mathbf{x}, \sigma)$ knowing $\overline{\omega}(\mathbf{x})$. This happens since $n_1(\mathbf{x})$ and $n_2(\mathbf{x})$ are found from

$$n_1(\mathbf{x}) + n_2(\mathbf{x}) = 1\,, \qquad \omega_1 n_1(\mathbf{x}) + \omega_2 n_2(\mathbf{x}) = \overline{\omega}(\mathbf{x})\,. \tag{23}$$

The entropy S can thus be evaluated directly in terms of $\overline{\omega}(\mathbf{x})$:

$$S = \int \frac{[\omega_2 - \overline{\omega}(\mathbf{x})] \ln[\omega_2 - \overline{\omega}(\mathbf{x})] + [\overline{\omega}(\mathbf{x}) - \omega_1] \ln[\overline{\omega}(\mathbf{x}) - \omega_1]}{\omega_2 - \omega_1} d^2\mathbf{x} + \int \ln(\omega_2 - \omega_1) d^2\mathbf{x}\,. \tag{24}$$

A variety of $\psi_0(\omega_0)$ other than (22) can be derived as well. Assuming *a priori* that $\beta\mu(\sigma) = -|\sigma|/q$, that is, if the weight factor is Poissonian [40],

$$\omega_0(\mathbf{x}) = -2 \frac{\beta q^2 \psi_0}{1 - \beta^2 q^2 \psi_0^2}. \tag{25}$$

Assuming instead that $\beta\mu(\sigma) = -(\sigma/q)^2$, that is, if the weight factor is Gaussian [35, section VI D],

$$\omega_0(\mathbf{x}) = -\beta q^2 \psi_0 \,. \tag{26}$$

A primary importance has been attributed to the 'dressed vorticity corollary' (DVC) [35]. This corollary says that if one "guesses" n_0 from the macroscopical equilibrium state, that is if one writes $n_0(\mathbf{x}, \sigma) = \delta(\sigma - \omega_0(\mathbf{x}))$, then a frozen dynamics is obtained, which is the $\beta \to -\infty$ limit of the true one. It is to remark that the "dressed vorticity distribution"

$$g_d(\sigma) = \int \delta(\sigma - \omega_0(\mathbf{x})) d^2\mathbf{x} \tag{27}$$

is, in general, different from $g(\sigma)$. This $g_d(\sigma)$ will be approximated by the histogram of the vorticity distribution computed from a numerical simulation. While $g(\sigma)$ would be conserved by an inviscid dynamics, only $g_d(\sigma)$ may be constructed from the computed field, and will vary in time. Only at the initial time, by definition, $g(\sigma) = g_d(\sigma)$. A consequence of the DVC is that the equilibrium field ω_0 is the one that has maximal energy among all the fields with the same distribution $g_d(\sigma)$.

2.6 Applications of the maximum entropy theory

Several recent papers compare direct numerical simulations with the predictions of the maximum entropy theory. Even recognizing their value, we think that their Ansätze are not justifiable in our cases, or that their conclusions do not match our results. In detail, Miller, Weichman and Cross [35] take into account a two-valued (0,ω_0) and a three-valued (0,ω_0,$-\omega_0$) initial condition onto a circular corona with no slip boundaries. They solve the variational problem by a Montecarlo dynamics and compare it with a direct numerical simulation of the flow. Whitaker and Turkington [54] consider two equal circular vortex patches on a closed disk, with zero ambient vorticity.They use an iterative solver for the constraint equations, and compare the result with more extensive contour dynamics simulations on the infinite plane (not on the disk). Sommeria, Staquet and Robert [47] consider a shear layer, with periodical boundary conditions in the x direction and slip walls in y. Their simulation starts from a two-level initial condition ($\omega = 0, a$), and the nonlinear eigenvalue problem is solved accordingly. In a particular limit, they are able to compute analytical solutions, which exhibit a bifurcation in the parameter space. One of those branches corresponds to solutions which break the symmetry in x, but are stationary (except for a system of reference mean velocity). Their *a-posteriori* fit of the $\omega(\psi)$ scatterplot is satisfactory only for one tract of the complete

curve. They also mention simulations of multiple shear layers, saying that different local vortices are obtained, preventing the system to achieve a steady state ("the system tends to achieve local equilibria into vortices faster than the global equilibrium"). Additional simulations of an idealized jet are done by Thess, Sommeria and Jüttner [48]; also in that case x-symmetry breaking solutions are found from the maximum entropy theory, and a better quantitative match is obtained. Symmetry breaking for periodic square, periodic channel and box boundary conditions is further discussed along those lines in a subsequent paper [22].

In the maximum entropy setting, continuous symmetries generate additional terms in the exponentials of the equations (19). If these terms involve an explicit dependence on the coordinates, such as in the case of the conserved angular momentum on the infinite plane, the soultion of (19) could be non stationary [44]. In the periodic case, however, no continuous symmetry besides the translation exists, and this possibility is prevented.

Chavanis and Sommeria [14] start assuming that $\omega(\psi)$ is linear, as it is in the minimum enstrophy context, and give analytical maximum entropy solutions for rectangular and circular closed domains. This is said to be justifiable in a particular 'strong mixing' limit. The solutions are always stationary, but admit monopole/multipole bifurcations, which are thoroughly listed.

A true attempt to validate the maximum entropy rather than the minimum enstrophy theory in an experiment is done by Huang and Driscoll [20]. They consider a rather simple metaequilibrium profile of a magnetized electron column, which obeys to the 2D Euler equation. They conclude that the mixing cannot be assumed to be ergodic and that the closest fit to the data is provided by the numerical minimum enstrophy solution.

3 Numerical experiments

We performed a number of numerical experiments. To this extent we integrated in time several vorticity fields, using a rather standard protocol for the Navier–Stokes equation. We used a two-dimensional 2/3 dealiased pseudospectral code on the periodical square $(2\pi)^2$. This choice, which fixes the Green function of the problem, was done for easiness of implementation. Nothing in the previously exposed theories prevents us to use this particular choice of boundary conditions. The Green function becomes $G(\mathbf{k}) = 1/k^2$ in Fourier space, as known. The (undealiased) resolution of the vorticity fields considered ranges between 16^2 and 512^2. A small viscosity is introduced mainly for numerical purposes, in order to prevent finite size effects, such as high wavenumber pile-up. Viscosity is seen to be too small if the energy, as seen from the $E(k)$

spectrum, accumulates at high k. According to a generally accepted practice, we used hyperviscous dissipative terms of the form $\nu_2\nabla^4\omega$ or $\nu_3\nabla^6\omega$ in place of the ordinary viscous term. Even if drawbacks in the use of hyperviscosity instead of normal viscosity have been recently discussed [21], we think that the choice is in practice uninfluent to our simulation. We confronted runs in which the same initial conditions were integrated with different forms of the dissipative term, observing almost no influence on the resulting final configuration. The small scale character of the hyperviscosity suppresses also some truncation effects, such as Gibbs wiggles in the proximity of steep gradients of the vorticity. Some dissipation is needed to 'underresolve smoothly' the smallest features which form during the evolution. The amount of dissipation has to be grossly matched with the rate of creation of smallest-scale structures, but does not have to be fine tuned. Time marching is accomplished by a fourth order Runge-Kutta integrator, with explicit treatment of the dissipative term. A Courant–Friedrichs–Levy condition is employed to vary the time-step. The adoption of $\Delta t = 0.3\Delta x/|\mathrm{v}_{\max}|$ appears to be accurate enough.

Most of our runs started from initial conditions consisting of variously arranged constant patches of vorticity. In most cases we simply distributed equal areas of vorticity equal to ± 1 on the square. This already provided us with quite a variety of outcomes, and allows direct connection with the various formulas of section 2. A pattern of this sort is the family of the 'fuzzy checkers'. By these we mean checkers with randomly perturbed edges. The perturbation is done in a way that insures a constant zero mean vorticity. A regular checker of vorticity is an unstable stationary field (the velocity is orthogonal to the gradient of vorticity, which is significantly different from zero only on the boundaries), while 'fuzzy' checker is immediately destabilized. Another possibility to generate (usually) unstable initial conditions, is to consider random arrangements of rectangular $\omega = \pm 1$ tiles upon the domain. A little smoothing on the initial conditions is actually necessary to prevent the edge ringing mentioned above, but, again, it does not seem critical for the results. As remarked above, those initial conditions, even if a little odd in appearance, are perfectly legitimate as test cases for the relaxation models. The resolutions of the various runs presented, together with the hyperviscous coefficient ν_3, the total integration time T_f, the initial and final values of energy and enstrophy E_0, E_f, Q_0 and Q_f, are reported in Table 1.

A typical case is shown in figure 1. The patches initially intertangle in a complicate way. The process generates a lot of filamentary features, which, both because of the finite resolution and the small-scale dissipation, are blurred out and disappear from the landscape. At later times, the final shape becomes apparent. The process of stretching and uniformization of the details continues, and a 'simpler' state stabilizes. This configuration undergoes no further evolution, apart of a slow erosion of its contours, due to the viscosity. Since the viscosity can in principle be made very small, this state is long lived and

Fig.	res.	ν_3	T_f	E_0	E_f	Q_0	Q_f	$\diamond$	$\equiv$
1	400^2	$4 \cdot 10^{-13}$	449	.01078	.01072	.457	.015	+14%	−6.1%
2	256^2	$2 \cdot 10^{-11}$	745	.1052	.1051	.455	.107	+.26%	−10%
	64^2	$4 \cdot 10^{-8}$	660	.119	.117	.36	.12	+.17%	−11%
	256^2	$2 \cdot 10^{-11}$	741	.0138	.0135	.48	.018	+2.7%	−19%
	64^2	$4 \cdot 10^{-8}$	1047	.034	.032	.319	.037	−.04%	−20%
	64^2	$1.9 \cdot 10^{-8}$	1291	.0107	.0082	.431	.012	+2%	−30%
	256^2	$2 \cdot 10^{-11}$	343	.16458	.16454	.29	.20	+.6%	−16%
4	128^2	$2 \cdot 10^{-9}$	704	.0178	.0169	.386	.022	+1.8%	−14%
	256^2	$2 \cdot 10^{-11}$	219	.16417	.16406	.427	.169	−.5%	−2%
	256^2	$5 \cdot 10^{-12}$	267	.1329	.1328	.466	.144	−1.2%	−4.8%
	64^2	$4 \cdot 10^{-8}$	182	.3963	.3961	.445	.433	−12%	+1.4%
5	256^2	$2 \cdot 10^{-8}$	165	.1639	.1629	.418	.184	−8%	+5.9%
	256^2	$2 \cdot 10^{-9}$	175	.1639	.1634	.418	.184	−9.4%	+4.3%
	256^2	$2 \cdot 10^{-10}$	228	.1639	.1637	.418	.186	−8.6%	+5.2%
	256^2	$2 \cdot 10^{-11}$	293	.1639	.1638	.418	.187	−11%	+3.5%
7	512^2	$4 \cdot 10^{-12}$	340	.1991	.1991	.486	.213	−4.5%	+3.7%
	256^2	$2 \cdot 10^{-11}$	208	.1991	.1990	.487	.213	−4.8%	+3.5%
	64^2	$4 \cdot 10^{-8}$	367	.199	.198	.486	.202	−3.5%	+1.1%
	32^2	$2 \cdot 10^{-7}$	419	.199	.196	.467	.199	−1.5%	−.2%
	16^2	$1 \cdot 10^{-6}$	907	.198	.190	.408	.191	−1.3%	−3.9%

Table 1
Resolution, hyperviscous coefficient ν_3, total integration time T_f, initial and final values of energy and enstrophy E_0, E_f, Q_0, Q_f for the runs presented. The last two columns give the increase in energy of the "prototype rearrangements" described in Appendix A.3, relative to E_f. $\diamond$ stands for the 'square dipole' and $\equiv$ for the 'smooth stripe'.

can be named 'final'. At this stage, the viscous term of equation (1) is some orders of magnitude smaller than the vorticity (or the strain) field, everywhere on the domain. The evolution of the velocity field is therefore still dominated by the nonlinear terms, which balance to make the convective term null and the vorticity configuration stationary. The timescale for viscous damping is much longer than the characteristic turnover time.

In the case of figure 1 the final state is a dipole. Something similar is also observed in other cases. We document a few of them in figure 2. The broadest

vorticity contours in the final state appear squared because of the bi-periodic boundary conditions. This reflects the shape of the Green function [18,46]. The maximum and the minimum of vorticity are unique, and displaced each other by half of the box size in both coordinates. The final state is stationary, and this agrees with the traditional point of view, but not entirely. The profiles of the positive and negative cores may differ. The scatterplot of (ω, ψ) tends to a line, but does not match any of the expected functional relations, such as (8), (13) or (22). In all cases, the scatterplot of (ω, ψ) is seen to lie in the first and third quadrants. This is consistent with any of the proposed $\omega(\psi)$ relations, in which β is negative. In addition, the different cases mix differently the available vorticity. If we plot the global distribution of the vorticity (third panels of the graphs in figure 2), we see that the final histograms vary from case to case. The profile of the final vortex cores is therefore peculiar to each decay. In all of them, however the final vorticity has a single maximum and sigle minimum, and the dipole may be thought as an arrangement of the avaliable vorticity around two centers.

The final dipole is not the only possibility, though. In figure 3, we see a different outcome. In this case a pattern of two stripes is formed. The boundaries of these two stripes translate in opposite directions varying slightly their curvature according to their relative position. The state is therefore recurring. Interestingly, the two zones cannot be explained simply by the absence of mixing of the original patches: detailed analysis shows that each stripe contains a fraction of the fluid of originally opposite vorticity. The mixing inside a single stripe is complete, so that the vorticity is almost constant and lower than that of the likely-colored patch in the initial condition. The effectiveness of mixing within the stripe, but its absence among the two stripes, is clearly evidenced when including numerical passive markers into the flow (figures omitted).

In figure 4 we see other examples of fields which decay in nonstationary final states. There is a variety of forms: non-symmetric fat cores, which oscillate in time; wavy stripes with central blobs that translate in one direction. Yet the last case shown in figure 2 is not really a simple dipole; actually three smaller and long lived vortices happen to form inside the main core. They keep orbiting for long time and weaken very slowly because of the viscosity, but are never able to merge. It is sometimes common, as in the case of figure 3, to get a complete uniformization of the vorticity in different well-separated zones of the flow. A number of patches of almost constant vorticity are thus formed, and their arrangement prevents further mixing. In all these cases the scatterplot of (ω, ψ) never thins out, and, *a fortiori* cannot be fitted by any of the relations given in section 2. Nevertheless, these configurations are long lived. Several features are still common to both types of decays. The final states are "dipoles" in a broad sense, in that they show two simply connected regions of vorticity above and below the mean. The local maxima of $|\omega|$ are

also absolute maxima. The small-scale structures are generated (and subsequently blurred) quite early in the simulation. If we compute characteristic eddy turnover times based on the sizes of the patches in the initial conditions, we see that the palinstrophy (associated to the amount of details) reaches its maximum within a few turnarounds. The entire simulation is carried on typically for some tens of turnover times. The loss of energy during the decay is always negligible. The enstrophy is seen to decay significantly during the decay, until the final state is formed; it then remains nearly constant. Most of the theories proposed in section 2 take into account a lowering of Q, but fix it in an unique way. We see that not even the initial E *and* Q are sufficient to determine the final state: as a counterexample, the case of figure 3 and the one shown in the second row of figure 4 possess initially nearly the same values of E and Q, and the same distribution of vorticity, but reach different final states. Other counterexamples may be easily generated taking an intermediate configuration and reversing the time integration. The blurring of details is an irreversible process, and the backward integration does not lead back to the initial condition. The forward and backward final states have generally different properties.

For the initial conditions we have used, the final states appear to be quite independent from the resolution and the (small) values and forms of the viscosity. Generally, a higher spatial resolution just requires a longer time to finish to smooth the details and to reach the final state. To ground this affirmation we give some examples.

First, we repeated the simulation shown in figure 3 with four different values of the hyperviscosity. The appearance of the field after long times is shown in figure 5. The same wavy pattern, with uniform stripes of vorticity and undulated boundaries is seen. Phase differences between the final panels are not meaningful, since the field is plotted at different times. To demonstrate the convergence and to provide one example of the evolution in time of the characteristic quantities, we plot, in figure 6, $E(t)$, $Q(t)$ and $P(t)$ for the different values of ν_3. The functions E and Q always stabilize on the final level. The loss in E is indeed negligible, less than 1% in the most dissipated case. The enstrophy instead decreases of roughly a factor two, but stabilizes to a final value independent of the hyperviscosity. The palinstrophy is seen to increase in time in the initial stages. This behavior, which is also predicted by closure theories' estimates, is related to the increase of small-scale details. The maximum value is achieved when such details begin to be more rapidly numerically underresolved than generated. This can be seen by looking at the field in physical space (compare for instance the intermediate panels of figure 3). The curves are also seen to scale inversely to the hyperviscosity. This behavior, apart from different values and different relaxation times, is also found in all the other decays, both the stationary and nonstationary ones. It is also observed when normal viscosity or second viscosity are employed.

Secondly, in order to show that the final state found is not an artifact of the finite resolution, we display the integration of another arbitrary initial condition at different spatial resolutions (figure 7). The hyperviscosity coefficients are adjusted case by case according to the highest wavenumber retained. We see that unless the resolution is extremely poor (16^2), a final state with given characteristics is obtained. In this case, the final state is nonstationary, the two elongated cores translate in one direction, while both background stripes convect in the opposite one.

We note, passing by, that the Fourier spectrum of these final states is always decreasing in k. We are not however concerned with possible laws to fit their slopes, and we do not report them here. In general, the final state is neither a pure $|\mathbf{k}| = 1$ state (as predicted by the minimum enstrophy principle), nor a spectrum introduced in section 2.1. Most of the energy of the final field is contained in the first modes, but this fact itself does not explain the formation of a huge variety of profiles.

4 Conclusions and perspectives

We have considered several examples of relaxations of two-dimensional vorticity fields, and compared them with the theories which have been so far proposed in literature. We have brought some numerical evidence that contrasts with the existing final states theories. The different theories do not agree in their predictions, as can be seen in the different $\omega_0(\psi_0)$ which they propose. We have shown the existence of legitimate final states which are not included in the accepted point of view. Nonstationary ones are among them. The remark that stable, nonstationary configurations may indeed form from unstable ones is indeed not new. Stable tri- and quadrupole satellite systems, which result from the decay of unstable vortex blobs, have already been investigated analytically and numerically [13,12,38,11]. Beautiful experimental evidence is also provided [52,17]. In all these cases (ω, ψ) is derived from the experiment, and is seen to evolve from a non-monotonous to a branched monotonous curve. On the other hand, also the non-uniqueness of stable dipolar solutions on the periodic box has been stressed [42]. Numerical experiments shown there display (ω, ψ) scatterplots which are tentatively fitted by polynomial relations. For this reason we have not tried to fit one or the other of the free parameters of the reported models versus our numerical results: the possibility of a good fit appears more accidental than general. In our opinion many of the underlying assumptions of these theories are not always granted, and call therefore for a more careful treatment. For instance, we think that the final state cannot be predicted by a 'final state theory' which ignores completely the dynamical path underwent by the relaxing system. This is demonstrated by the fact that configurations with the same two initial vorticity levels decay to different final

states. The quest for appropriate statistical descriptors, which are preserved during the evolution, is still open. For instance, it is not known how the initial macrovorticity distribution relaxes to the final one. It would be appealing to parametrize this change by a few dynamical quantities, such as the decrease of Q. We have supposed that some of the shapes of the final states can be understood as rearrangements of the vorticity which is available at late times. This seems to apply at least to the final stationary states, for which the requirement of energy maximization appears as sufficient. The instability of the intermediate vorticity configurations is always such that the system is led to mix its vorticity and drawn toward the final state. In the other cases we may conjecture that, for some stability reason, the available vorticity is unable to collapse onto a stationary configuration. In many of the previous works, initial Gaussian fields with random spectra were considered. These fields show generally a smaller population of absolute higher vorticity (i.e., $g_d(\sigma)$ with long tails). It is often observed (but not always ([3,25]) that a lot of concentrated vorticity patches are formed in the early times of evolution and they survive relatively long times. Such intermediate states, composed of several isolated cores, which have so often been described in literature, could be understood as metastable preliminary local rearrangements of the vorticity.

In other cases, however, the attainment of stationary states seems prevented. Possibly, the system is trapped in a metastable state, which is not stationary (in the cases encountered in this work, periodical in time). The stationary state could be missed just because the dynamics of the vorticity is by itself insufficient to trigger a catastrophic mixing process, which alone could alter further the vorticity distribution, and lead the system to its very final state. It would then be very interesting to find the requirements for this metastability. An implication of such metastabilities would be that some kind of external forcing might trigger the transition to the stabler states and some perhaps not.

Acknowledgements

The motivation of this work originates from discussions with Professors R.A. Pasmanter and K. Ohkitani while one of the authors (S.K.) visited the Koninklijk Nederlands Meteorologisch Institut, under the support provided by the Dutch Science Foundation NWO, Priority Programme on Nonlinear Dynamical System. The major part of this work was then carried on at the Research Institute for Mathematical Sciences of the University of Kyoto. E.S. was supported during that period by the Japanisch-Deutsches Zentrum Berlin Sonderaustausch Program. We would like to express our gratitude to Prof. R. Pasmanter, Prof. K. Ohkitani, Dr. G. Boffetta and Dr. A. Celani for their comments and fruitful discussion.

Appendix: Energy maximization and stability

All the theories proposed in section 2 identify the final state as the one which solves a certain extremum problem. In the case of the minimum enstrophy principle, one may think to rescale the vorticity, and to rephrase the problem as to the search for the maximal energy, given a fixed enstrophy. In the setting of the minimum entropy, the DVC instead tells us that the final state is actually also a state of maximal energy (with fixed g_d). It is therefore worth to add some remarks on energy maximization.

We are not able to determine in how many equally energetic ways the same amount vorticity can be distributed over a domain. We might ask if equally energetic states which are not dynamically related, i.e., which do not evolve one into the other, because they are topologically different, could converge to the same final state. We cannot answer to those questions, but we can add a few considerations which at least rule out some possibilities. These provide necessary requirements, but they do not determine the configuration of vorticity nor the flow.

A.1 Infinitesimal deformations

Let us first consider a generic area preserving infinitesimal deformation on a two-dimensional domain. The deformation may be written as $\delta\mathbf{x} = \nabla^{\perp}\delta\phi(\mathbf{x})$, where ϕ is an arbitrary field. It is easily seen that such transformations preserve all the moments of the vorticity:

$$\begin{aligned}\delta\int\omega^l d^2\mathbf{x} &= l\int J(\omega,\delta\phi)\omega^{l-1}d^2\mathbf{x} = \\ &= -l\int\delta\phi\left[(\omega_x\omega^{l-1})_y-(\omega_y\omega^{l-1})_x\right]d^2\mathbf{x}=0,\end{aligned} \tag{28}$$

Integration by parts is carried out since the boundary terms vanish for any boundary condition. The variation of the energy with respect to such deformations is

$$\begin{aligned}\delta E &= \delta\tfrac{1}{2}\int\omega(\mathbf{x})\omega(\mathbf{x}')G(\mathbf{x}',\mathbf{x})d^2\mathbf{x}d^2\mathbf{x}' = \int\delta\omega(\mathbf{x})\omega(\mathbf{x}')G(\mathbf{x}',\mathbf{x})d^2\mathbf{x}d^2\mathbf{x}' = \\ &= -\int J\left(\delta\phi(\mathbf{x}),\omega(\mathbf{x})\right)\omega(\mathbf{x}')G(\mathbf{x}',\mathbf{x})d^2\mathbf{x}d^2\mathbf{x}' = \\ &= \int\delta\phi(\mathbf{x})J\left(\omega(\mathbf{x}),G(\mathbf{x}',\mathbf{x})\right)\omega(\mathbf{x}')d^2\mathbf{x}d^2\mathbf{x}'.\end{aligned} \tag{29}$$

Therefore the extremal energy states satisfy

$$\frac{\delta E}{\delta \phi} = \int J\left(\omega(\mathbf{x}), G(\mathbf{x}', \mathbf{x})\right) \omega(\mathbf{x}') d^2\mathbf{x}' = J\left(\omega(\mathbf{x}), \psi(\mathbf{x})\right) = 0. \tag{30}$$

Thus if the dissipation is absent, the stationary states extremize the energy with respect to infinitesimal incompressible deformations. These states are "local" extrema.

A.2 Pointwise mixing exchanges

We can write a transformation which transfers some of the vorticity present in the neighborhood of $\mathbf{x}_1$ to a similar neighborhood of $\mathbf{x}_2$ and vice versa. To this extent we employ a shape function $\delta_\epsilon(\mathbf{x})$, which is equal to 1 in a neighborhood of radius ϵ of $\mathbf{x} = 0$ (modulo the boundary conditions) and zero everywhere else. The vorticity field is transformed according to

$$\begin{aligned} \omega(\mathbf{x}) \to \omega(\mathbf{x}) &+ r\left[\omega(\mathbf{x} - \mathbf{x}_1 + \mathbf{x}_2) - \omega(\mathbf{x})\right] \delta_\epsilon(\mathbf{x} - \mathbf{x}_1) \\ &+ r\left[\omega(\mathbf{x} + \mathbf{x}_1 - \mathbf{x}_2) - \omega(\mathbf{x})\right] \delta_\epsilon(\mathbf{x} - \mathbf{x}_2). \end{aligned} \tag{31}$$

The parameter r may vary from 0 to 1; in the latter case, an exchange between the vorticity in $\mathbf{x}_1$ with that in $\mathbf{x}_2$ is realized. The energy of the transformed field is computed by substituting the above expression in equation (3). When consider the limit $\epsilon \to 0$, the integrals are approximated by the mean value of the integrand times the area of the integration region, provided that ω is continuous. The terms multiplied by r come of order $O(\epsilon^2)$, while the ones with r^2 remain $O(\epsilon^4)$. The singularity in the Green function poses no problems, since for small arguments $G(\mathbf{x}, \mathbf{y}) \sim -\ln|\mathbf{x}-\mathbf{y}|$, which is integrable. Therefore

$$E \to E + r\pi\epsilon^2[\psi(\mathbf{x}_2) - \psi(\mathbf{x}_1)][\omega(\mathbf{x}_1) - \omega(\mathbf{x}_2)] + r^2 O(\epsilon^4). \tag{32}$$

This gives us the infinitesimal change in energy due to a transformation which modifies infinitesimally, but not continuously, the field. The fact that this transformation is not dynamical is not of our concern, as far as we look for properties of the configurations and not for their evolution.

If we refer to the maximal energy state, its energy shall decrease whichever the couple of points $\mathbf{x}_1$ and $\mathbf{x}_2$ and the value of r. Therefore, $\omega(\mathbf{x}_2) > \omega(\mathbf{x}_1)$ implies $\psi(\mathbf{x}_2) > \psi(\mathbf{x}_1)$ and vice versa. The most important consequence of it is that $\psi(\omega)$ must be single valued and monotonous. This is seen by considering the plot of $\omega(\mathbf{x})$ versus $\psi(\mathbf{x})$. The monotonicity is implied by the fact that data points on the (ω, ψ) plane can be labelled by $\mathbf{x}$. If the relation $\omega(\psi)$

was non monotonous or more than single valued, then it would be possible to find points at which $\omega(\mathbf{x}) = \omega(\mathbf{x}_1)$ and $\psi(\mathbf{x}) > \psi(\mathbf{x}_1)$. Excluding degenerate cases, such as $\psi(\omega)$ nowhere differentiable or a vertical tangent to the curve $\omega(\psi)$, there would also exist points $\mathbf{x}_2$ close to $\mathbf{x}$ such that $\omega(\mathbf{x}_2) < \omega(\mathbf{x}_1)$ but still $\psi(\mathbf{x}_2) > \psi(\mathbf{x}_1)$, contrary to the hypothesis As a further consequence, the absolute maximal energy state is also stationary, because $\omega(\mathbf{x})$ and $\psi(\mathbf{x})$ are functionally related.

A particular case is achieved when the the points are infinitesimally close and displaced in the direction $\mathbf{d}$: in this case (32) is read as $(\mathbf{d} \cdot \nabla\psi)(\mathbf{d} \cdot \nabla\omega) > 0$ at any point and along any direction.

Related to this, but derived with a different machinery, is the Rayleigh–Arnold criterion [19,32,10]. It states that among all the isovortical fields the maximal energy arrangement is unique and stationary. Furthermore, if $d\psi_0(\omega_0)/d\omega_0$, or equivalently $-\nabla\psi_0 \cdot \nabla\omega_0/|\nabla\omega_0|^2$ are strictly positive and limited, then the field is also nonlinearly stable. We also note that there may exist also other stable states, in particular those obtained by means of some symmetry transformation, which is specified by invariants inexpressible as functionals of the vorticity. Analytical stability criteria other than Arnold's one, that refer to local features in ambient flows (e.g. [39]), do not appear to be of direct use for assessing global stability.

A.3 Energy maximization algorithms

We have seen in A.1 and A.2 properties of 'energy-maximizing arrangements of the available vorticity'. By 'arrangement', we mean another field, which has exactly the same fractional area for each level of vorticity (i.e. the same vorticity histogram), but a different configuration. The preceding facts tell us that these rearrangements are unique, stationary and stable. We are not, however, guaranteed that *any* initial field relaxes into such an energy maximizing configuration. Not only it is *a priori* undetermined how the histogram of macrovorticity evolves in time, but also not all fields are seen to approach a stationary final state. We want therefore to characterize the maximal energy state for a given vorticity population, and its relation with the observed dynamical final state.

One possibility would be provided by the Carnevale, Vallis and Young pseudo-dynamics [50,10]. They proposed a numerical procedure to deform a vorticity field by increasing its energy and conserving its enstrophy. The procedure does not explain the geometrical properties of the extremal states, which can only be said to be local, and not absolute maxima of the energy. Lacking analytical procedures, we rather used a simpler alternative combinatorial approach.

Starting from a given configuration of vorticity, two square tiles are randomly exchanged and the new energy is computed. The new configuration is kept if the energy increases, discarded otherwise, and the process repeated. Miller, Weichman and Cross [35] also use a more sophisticate numerical procedure of this kind. Such approach is easy to implement, but very slow in convergence when the number of tiles is significant. With the aid of this tool, we observed that the highest energy configuration achieved by permutation of equal area tiles of vorticity $\pm\omega_1$ on the periodic square, is a subdivision in two stripes parallel to the sides. When intermediate levels of vorticity are present, as in our runs, where patches' edges are significantly smoothed, the most energetical of these permutations of tiles has sometime still a striped shape, sometimes a central cored appearance.

To cope with high resolution rearrangements, we chose to limit ourselves to compare energies of only a few selected prototypical configurations. To produce them we sorted the discrete tiles of the field according to value of their vorticity, and deployed them upon the domain following the same order of a sample configuration. In this way we obtain a rearrangement with the same set of contour lines of a given prototype. We can then check which, among few prototype rearrangements, increases the current energy. One of the test profiles we chose is the "square dipole", which is modeled on $G(\mathbf{x}) - G(\mathbf{x} + (\pi, \pi))$; its contour lines look similar to those of various dipolar final states shown in Fig. 2. Another one is the parallel stripe, which is the maximal arrangement for a two-level population. If we compute the energies of the rearrangements of the final states obtained in section 3, we basically see that for the stationary final states the highest energy is achieved for the 'square dipole' rearrangement, with minimal increase of energy. For the nonstationary final states, such as the wavy ones, often the stripe rearrangement results more energetical. The actual values of the energies are reported in Table 1. The choice of the maximal profile is basically a function of the available vorticity. Still, the energy of the nonstationary states is often significantly increased by the procedure. This indicates that the final state, in those cases, is far from the highest energy configuration for the given g_d. Conversely, the final state may be dynamically inaccessible from the rearrangement: such is the case for the wavy configurations, if we maintain that the energy is almost conserved. In addition, the wavy cannot be seen as a perturbed stripe, since the maximal energy state cannot be unstable to transversal perturbations, thanks to the Arnold stability criterion.

We are not able to provide a full analytical treatment of the family of the recurring wavy solutions here, but we would like to add a small piece of numerical evidence. We plot the energy corresponding to all two level striped fields with sinusoidal undulations, with varying amplitudes and phase shift (figure 8). We see that the energy has to decrease significantly with increasing amplitude in order to allow for undulations of the boundaries. For a range of energies below

the highest, energy isolines span the entire interval $0 \leq \Delta\phi \leq 2\pi$, with the amplitude depending on the phase shift. A recurring evolution of the field, with pulsating amplitudes, is therefore allowed. Without attempting to make a precise fit to our final states, we claim that the picture is appropriate. It is clear from the figure that for amplitudes of the undulation higher than $A \sim \frac{1}{4}\pi$, but still lower than the geometrical limit $A = \frac{1}{2}\pi$, the range $0 \leq \Delta\phi \leq 2\pi$ is no more entirely accessible at constant E (the separatrix is drawn in bold). In fact, numerical tests with initial conditions of this kind exhibit stability below an amplitude threshold, and a catastrophic mixing above.

References

[1] P. Bartello and T. Warn. Self similarity of decaying two-dimensional turbulence. *Journal of Fluid Mechanics*, 326:357–372, November 1996.

[2] R. Benzi, S. Patarnello, and P. Santangelo. Self-similar coherent structures in two-dimensional decaying turbulence. *Journal of Physics A*, 21:1221–1237, 1988.

[3] M. E. Brachet, M. Meneguzzi, H. Politano, and P. L. Sulem. The dynamics of freely decaying two dimensional turbulence. *Journal of Fluid Mechanics*, 194:333–349, 1988.

[4] F. P. Bretherton and D. B. Haidvogel. Two-dimensional turbulence above topography. *Journal of Fluid Mechanics*, 78(1):129–154, 1976.

[5] E. Caglioti, P. L. Lions, C. Marchioro, and M. Pulvirenti. A special class of stationary flows for two-dimensional Euler equations: a statistical mechanics description. *Communications in Mathematical physics*, 143:501–525, 1992.

[6] L. J. Campbell and K. O'Neil. Statistics of two-dimensional vortices and high energy vortex states. *Journal of Statistical Physics*, 65(3/4):495–529, 1991.

[7] G. F. Carnevale. Statistical features of the evolution of two-dimensional turbulence. *Journal of Fluid Mechanics*, 122:143–153, 1982.

[8] G. F. Carnevale, J. C. McWilliams, Y. Pomeau, J. B. Weiss, and W. R. Young. Evolution of vortex statistics in two-dimensional turbulence. *Physical Review Letters*, 66(21):2735, May 1991.

[9] G. F. Carnevale, J. C. McWilliams, Y. Pomeau, J. B. Weiss, and W. R. Young. Rates, pathways, and end states of nonlinear evolution in decaying two-dimensional turbulence: Scaling theory versus selective decay. *Physics of Fluids A*, 4(6):1314–1316, June 1992.

[10] G. F. Carnevale and G. K. Vallis. Pseudo-advective relaxation to stable states of inviscid two-dimensional fluids. *Journal of Fluid Mechanics*, 213:549–571, 1990.

[11] X. Carton and B. Legras. The life-cycle of tripoles in two-dimensional incompressible flows. *Journal of Fluid Mechanics*, 267:53–82, 1994.

[12] X. J. Carton. On the merger of shielded vortices. *Europhysics letters*, 18:697–703, 1992.

[13] X. J. Carton, G. R. Flierl, and L. M. Polvani. The generation of tripoles from unstable axysymmetric isolated vortex structures. *Europhysics letters*, 9:339–344, 1989.

[14] P. H. Chavanis and J. Sommeria. Classification of self-organized vortices in two-dimensional turbulence: the case of a bounded domain. *Journal of Fluid Mechanics*, 314:267–297, May 1996.

[15] A. J. Chorin. *Vorticity and turbulence*. Number 103 in Applied mathematical sciences. Springer, 1994.

[16] G. L. Eyink and H. Spohn. Negative temperature states and large-scale, long lived vortices in two-dimensional turbulence. *Journal of Statistical Physics*, 70(3/4):833–886, 1993.

[17] J. Flor and G. van Heijst. Stable and unstable monopolar vortices in a stratified fluid. *Journal of Fluid Mechanics*, 311:257, March 1996.

[18] M. L. Glasser. The evaluation of lattice sums. III. phase modulated sums. *Journal of mathematical physics*, 15(2):188–189, February 1974.

[19] D. D. Holm, J. E. Marsden, T. Ratiu, and A. Weinstein. Nonlinear stability of fluid and plasma equilibria. *Physics Reports*, 123(1-2):1–116, 1985.

[20] X. P. Huang and C. F. Driscoll. Relaxation of 2d turbulence to a metaequilibrium near the minimum enstrophy state. *Physical Review Letters*, 72(14):2187–2190, 1994.

[21] X. Jimenez. Hyperviscous vortices. *Journal of Fluid Mechanics*, 279:169–176, 1994.

[22] B. Jüttner, A. Thess, and J. Sommeria. On the symmetry of self-organized structures in two-dimensional turbulence. *Physics of Fluids*, 7(9):2108–2110, September 1995.

[23] B. Jüttner, A. Thess, and B. Turkington. Statistical mechanics of two-dimensional turbulence. preprint, june 1996.

[24] S. Kida. Statistics of the system of line vortices. *Journal of the Physical Society of Japan*, 39:1395–1404, 1975.

[25] S. Kida. Numerical simulation of two-dimensional turbulence with high-symmetry. *Journal of the Physical Society of Japan*, 54:2840–2854, 1985.

[26] S. Kida, M. Yamada, and K. Ohkitani. The energy spectrum in the universal range of two-dimensional turbulence. *Fluid dynamics research*, 4:271–301, 1988.

[27] R. H. Kraichnan. Inertial ranges of two-dimensional turbulence. *Physics of Fluids*, 10:1417–23, 1967.

[28] R. H. Kraichnan. Inertial-range transfer in two- and three-dimensional turbulence. *Journal of Fluid Mechanics*, 47:525–35, 1971.

[29] R. H. Kraichnan and D. Montgomery. Two-dimensional turbulence. *Reports on Progress in Physics*, 43:547–619, 1980.

[30] C. E. Leith. Minimum enstrophy vortices. *Physics of Fluids*, 27(6):1388–1395, 1984.

[31] W. H. Matthaeus, W. T. Stribling, D. Martinez, and S. Oughton. Selective decay and coherent vortices in two-dimensional incompressible turbulence. *Physical Review Letters*, 66(21):2731, May 1991.

[32] M. E. McIntyre and T. G. Shepherd. An exact local conservation theorem for finite-amplitude disturbances to non-parallel flows, with remarks on Hamiltonian structure and on Arnold's stability theorems. *Journal of Fluid Mechanics*, 181:527–565, 1987.

[33] J. C. McWilliams. The emergence of isolated coherent vortices in turbulent flow. *Journal of Fluid Mechanics*, 146:21–43, 1984.

[34] J. C. McWilliams. The vortices of two-dimensional turbulence. *Journal of Fluid Mechanics*, 219:361–385, 1990.

[35] J. Miller, P. B. Weichman, and M. C. Cross. Statistical mechanics, Euler's equation and Jupiter's red spot. *Physical Review A*, 45(4):2328–2359, 1992.

[36] D. Montgomery and G. Joyce. Statistical mechanics of negative temperature states. *Physics of Fluids*, 17:1139–1145, 1974.

[37] D. Montgomery, X. Shan, and W. H. Matthaeus. Navier-Stokes relaxation to sinh-Poisson states at finite Reynolds numbers. *Physics of Fluids A*, 5(9):2207–2216, 1993.

[38] Y. G. Morel and X. J. Carton. Multipolar vortices in two-dimensional incompressible flows. *Journal of Fluid Mechanics*, 267:23–51, 1994.

[39] J. Nycander. Existence and stability of stationary vortices in a uniform shear flow. *Journal of fluid mechanics*, 287:119–132, March 1995.

[40] R. A. Pasmanter. On long-lived vortices in 2-d viscous flows, most probable states of inviscid 2-d flows and a soliton equation. *Physics of Fluids*, 6(3):1236–1242, March 1994.

[41] Y. B. Pointin and T. S. Lundgren. Statistical mechanics of two-dimensional vortices in a bounded container. *Physics of Fluids*, 19(10):1459–1470, October 1976.

[42] J. J. Rasmussen, J. S. Hesthaven, and M. R. Schmidt. Dipolar vortices in two-dimensional flows. *Mathematics and computers in simulation*, 40(3/4):207, April 1996.

[43] G. Riccardi, R. Piva, and R. Benzi. A physical model for merging in two-dimensional decaying turbulence. *Physics of Fluids*, 7(12):3091–3104, 1995.

[44] R. Robert and J. Sommeria. Statistical equilibrium states for two-dimensional flows. *Journal of Fluid Mechanics*, 229:291–310, 1991.

[45] R. Robert and J. Sommeria. Relaxation towards a statistical equilibrium state in two-dimensional perfect fluid dynamics. *Physical Review Letters*, 69(19):2776, November 1992.

[46] C. E. Seyler, Jr. Thermodynamics of two-dimensional plasmas or discrete line vortex fluids. *Physics of Fluids*, 19(9):1336–1341, September 1976.

[47] J. Sommeria, C. Staquet, and R. Robert. Final equilibrium state of a two-dimensional shear layer. *Journal of Fluid Mechanics*, 233:661, December 1991.

[48] A. Thess, J. Sommeria, and B. Jüttner. Inertial organization of a two-dimensional turbulent vortex street. *Physics of Fluids*, 6(7):2417–2429, July 1994.

[49] A. C. Ting, H. H. Chen, and Y. C. Lee. Exact solutions of a nonlinear boundary value problem: the vortices of the two-dimensional sinh-Poisson equation. *Physica D*, 26:37–66, 1987.

[50] G. K. Vallis, G. F. Carnevale, and W. R. Young. Extremal energy properties and construction of stable solutions of the Euler equations. *Journal of Fluid Mechanics*, 207:133–152, 1989.

[51] E. van Groesen. Time asymptotics and the self-organization hypothesis for the $2-D$ Navier-Stokes equation. *Physica A*, 148:312, 1988.

[52] G. van Heijst, R. Kloosterziel, and C. Williams. Laboratory experiments on the tripolar vortex in a rotating fluid. *Journal of Fluid Mechanics*, 225:301–331, April 1991.

[53] P. B. Weichman. Statistical mechanics, Euler's equation and Jupiter's red spot. In F. et al., editor, *Nonlinear waves and weak turbulence*, chapter 14, pages 239–277. Birkhäuser, 1993.

[54] N. Whitaker and B. Turkington. Maximum entropy states for rotating vortex patches. *Physics of Fluids*, 6(12):3963–3973, December 1994.

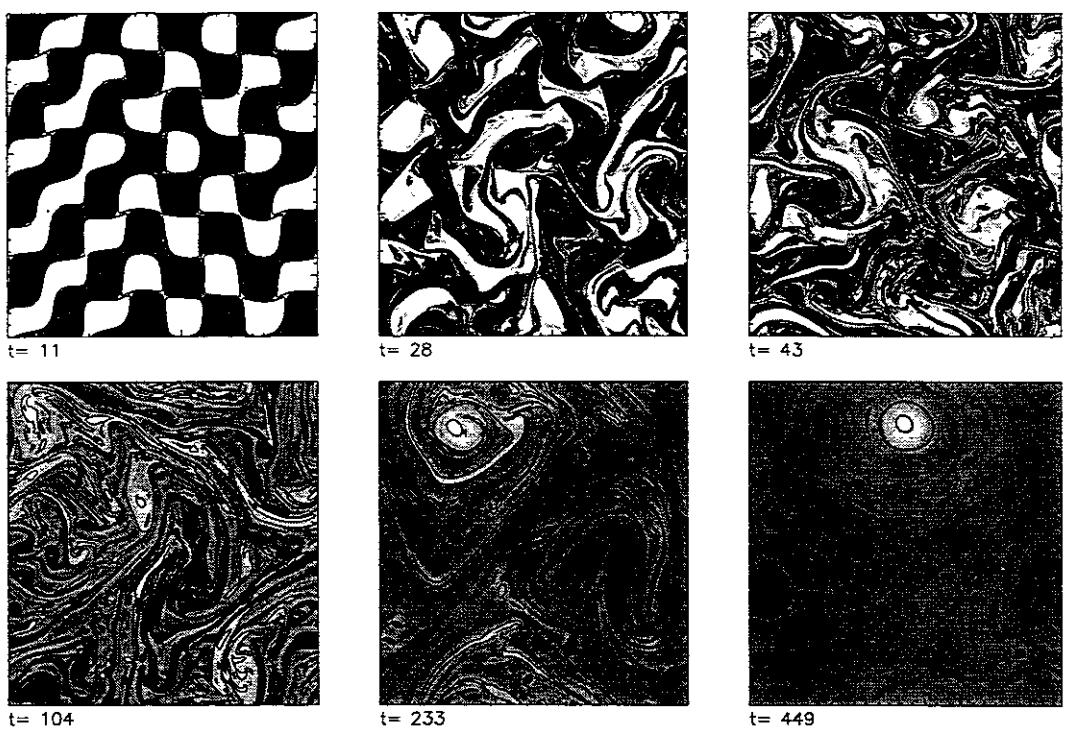

Fig. 1. A typical case: decay of a two-level patched vorticity field into a stationary dipole. Plots of the vorticity field at various times. A few vorticity isolines are drawn for reference.

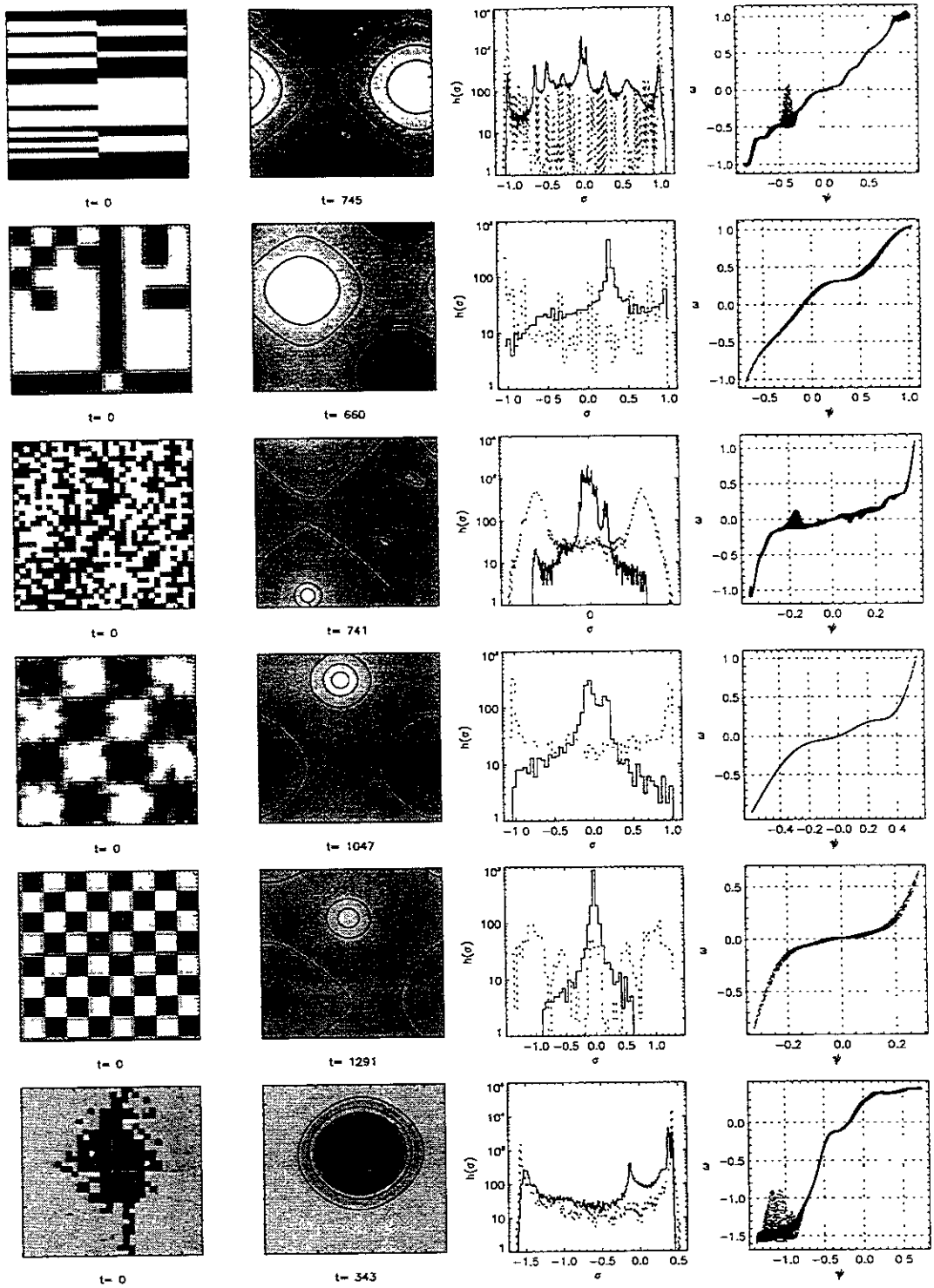

Fig. 2. Arbitrary 2-level initial conditions which decay in final dipoles. Each row illustrates one case, with, in each panel: the initial and the late time vorticity field; the initial (dashed line) and final (full line) global vorticity distributions; the final scatterplot of (ψ,ω). All cases start from initial patches with $\omega = \pm 1$, except for the last one, where $\omega = -1.5, +0.5$. The mean vorticity is always zero.

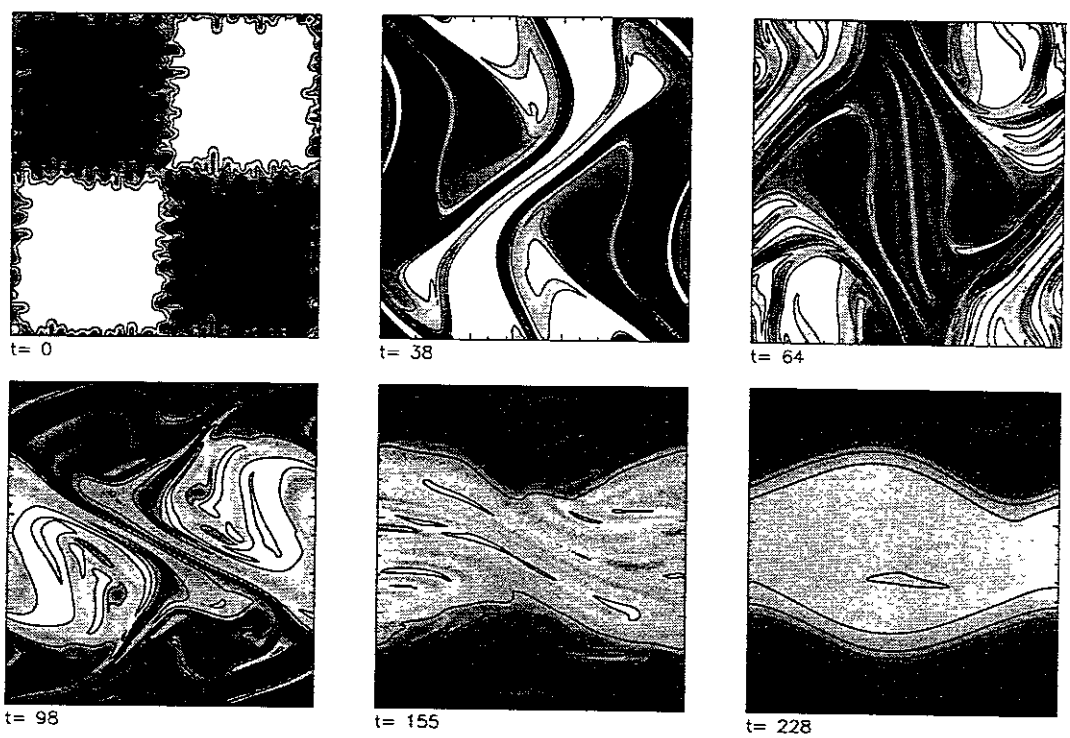

Fig. 3. A less typical case: decay of a two-level patched vorticity field into a wavy pattern.

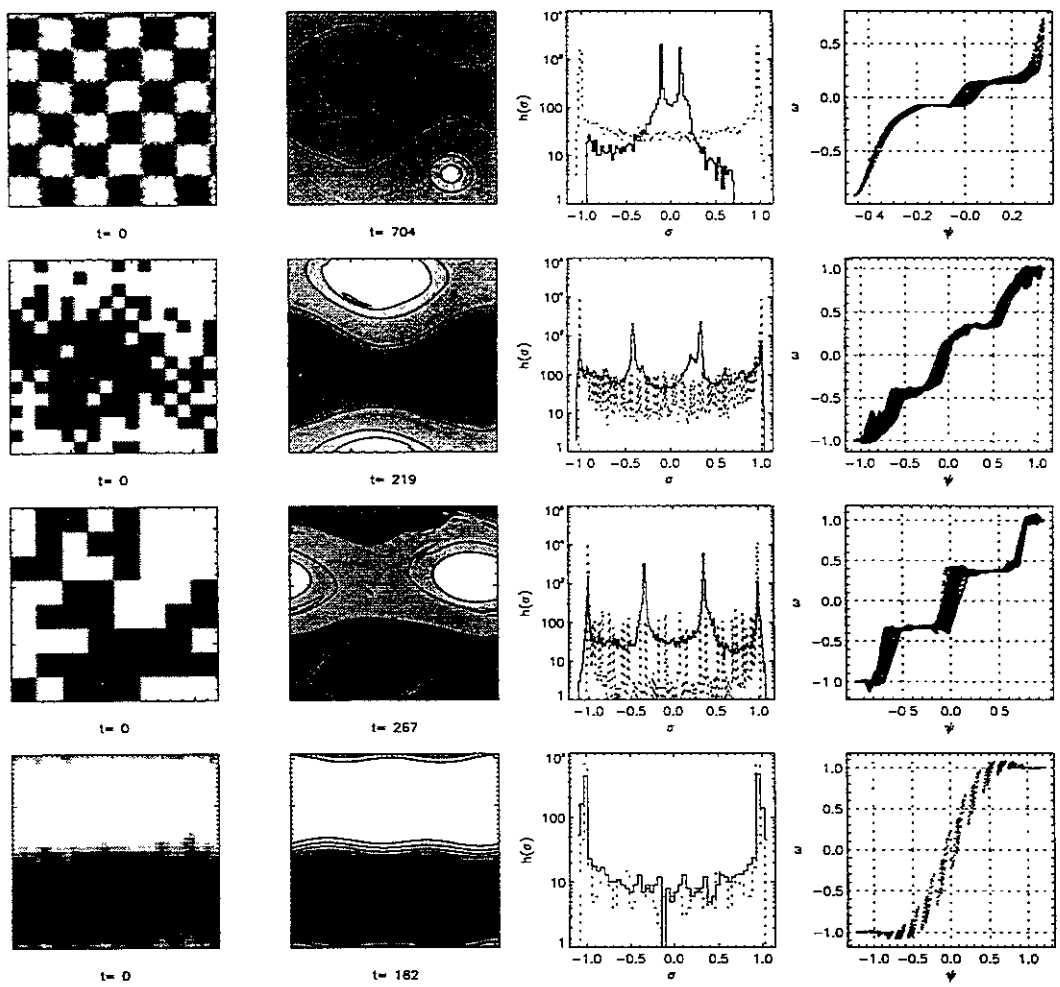

Fig. 4. Arbitrary 2-level initial conditions which decay in nonstationary configurations. The format of presentation is the same as in Fig. 2.

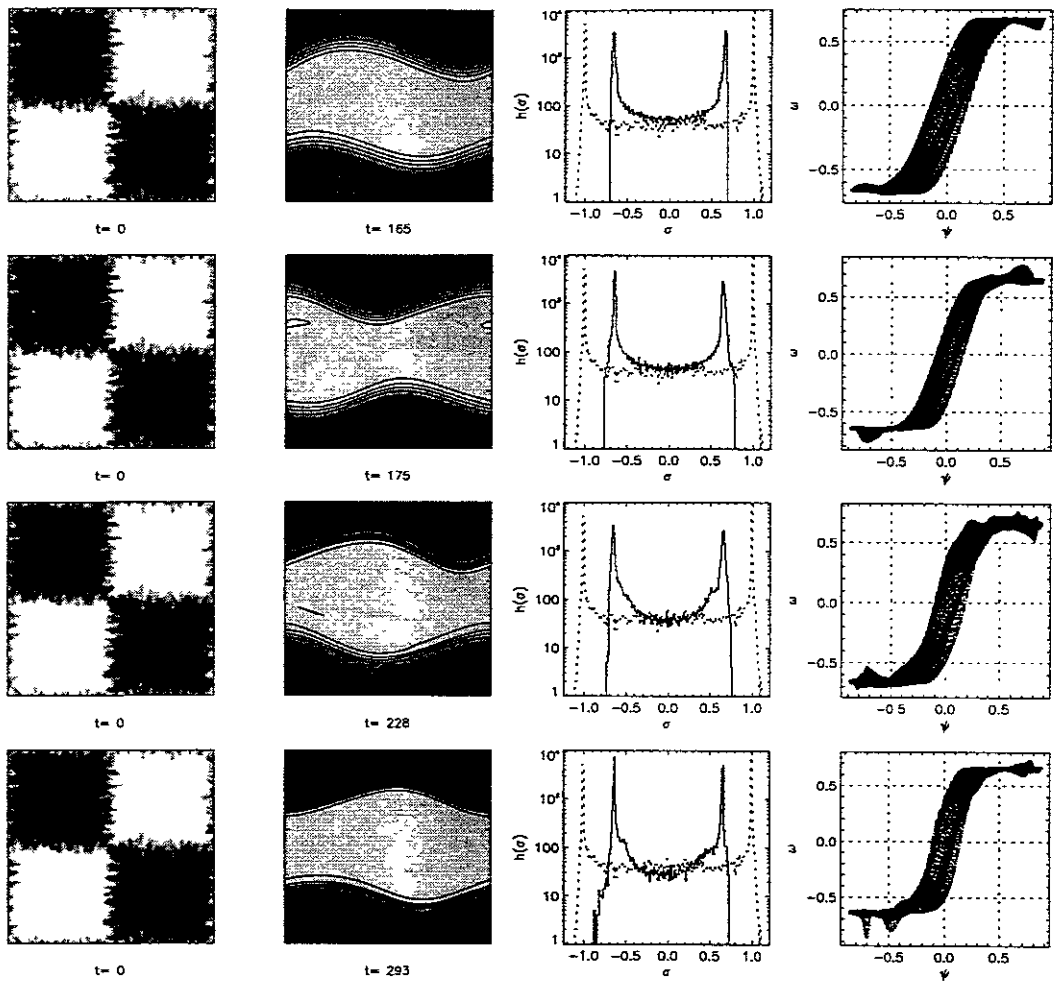

Fig. 5. Decay to the final wavy state, obtained with different hyperviscosities. The format of presentation is the same as in Fig. 2. The value of ν_3 is respectively $2 \cdot 10^{-8}$, $2 \cdot 10^{-9}$, $2 \cdot 10^{-10}$, and $2 \cdot 10^{-11}$.

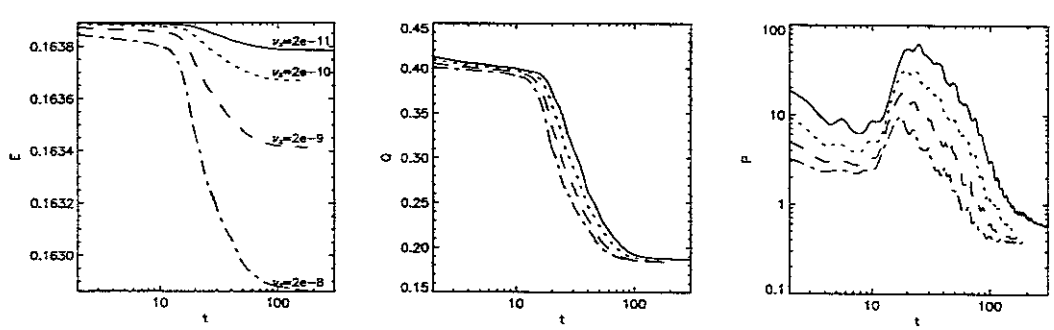

Fig. 6. Energy, enstrophy and palinstrophy decay for different values of the hyperviscosity.

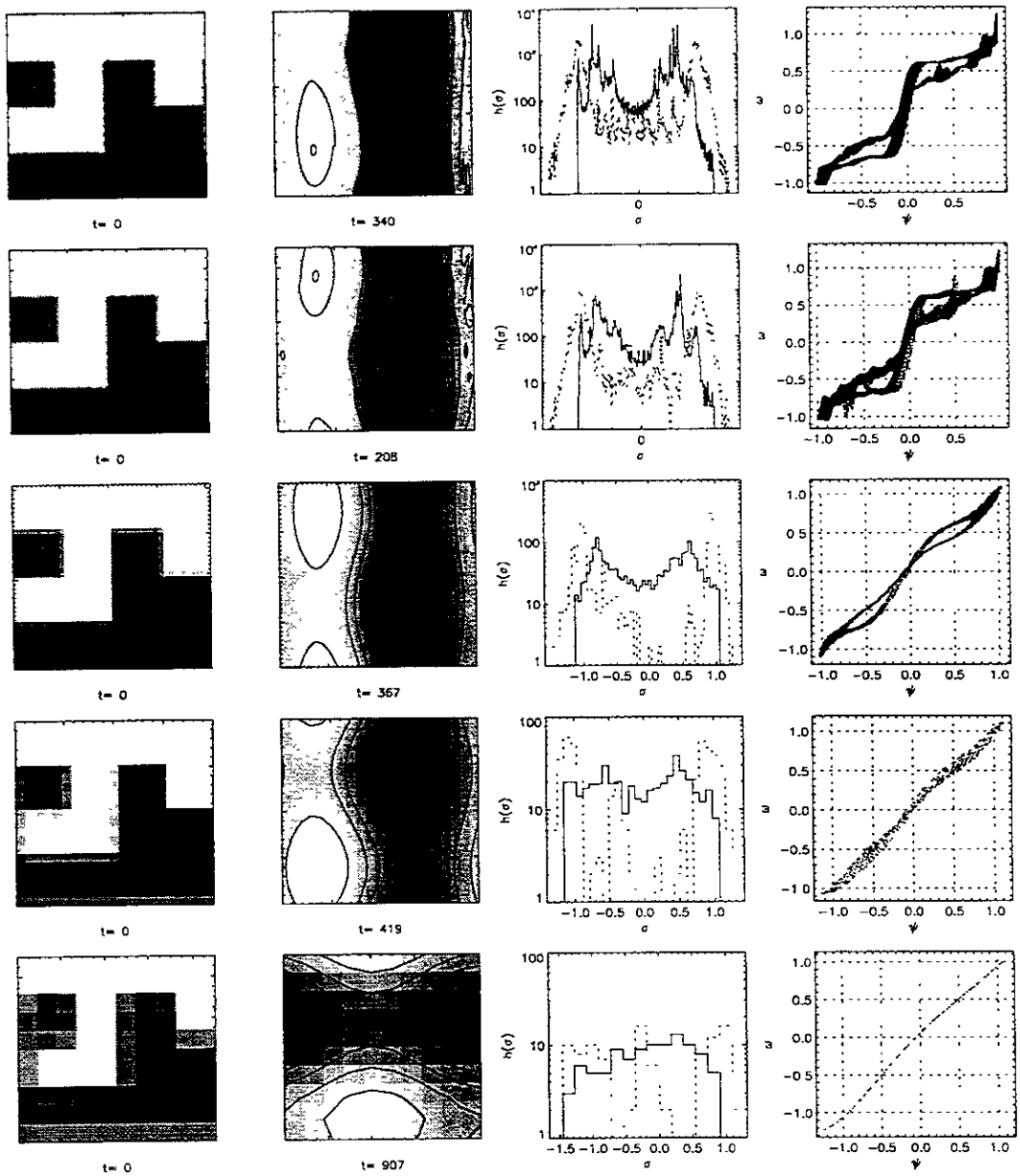

Fig. 7. Effect of lowering the resolution of the simulation. The same initial condition is integrated at 512^2, 256^2, 64^2, 32^2, 16^2, and hyperviscosity rescaled appropriately. The format of presentation is the same as in Fig. 2.

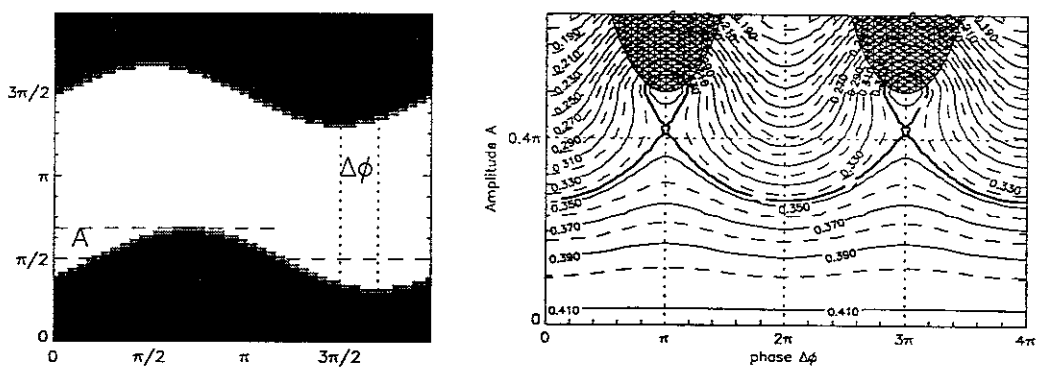

Fig. 8. Energy of a family of wavy patterns of vorticity equal to ± 1, as a function of A and $\Delta\phi$. The region of the $(A, \Delta\phi)$ plane where the two stripes would interfere is drawn cross-hatched.

Recent Issues of NIFS Series

NIFS-457 K. Itoh, S.- I. Itoh, A. Fukuyama and M. Yagi,
Turbulent Transport and Structural Transition in Confined Plasmas; Oct. 1996

NIFS-458 A. Kageyama and T. Sato,
Generation Mechanism of a Dipole Field by a Magnetohydrodynamic Dynamo; Oct. 1996

NIFS-459 K. Araki, J. Mizushima and S. Yanase,
The Non-axisymmetric Instability of the Wide-Gap Spherical Couette Flow; Oct. 1996

NIFS-460 Y. Hamada, A. Fujisawa, H. Iguchi, A. Nishizawa and Y. Kawasumi,
A Tandem Parallel Plate Analyzer; Nov. 1996

NIFS-461 Y. Hamada, A. Nishizawa, Y. Kawasumi, A. Fujisawa, K. Narihara, K. Ida, A. Ejiri, S. Ohdachi, K. Kawahata, K. Toi, K. Sato, T. Seki, H. Iguchi, K. Adachi, S. Hidekuma, S.Hirokura, K. Iwasaki, T. Ido, M. Kojima, J. Koong, R. Kumazawa, H. Kuramoto, T. Minami, I. Nomura, H. Sakakita, M. Sasao, K.N. Sato, T. Tsuzuki, J. Xu, I. Yamada and T. Watari,
Density Fluctuation in JIPP T-IIU Tokamak Plasmas Measured by a Heavy Ion Beam Probe; Nov. 1996

NIFS-462 N. Katsuragawa, H. Hojo and A. Mase,
Simulation Study on Cross Polarization Scattering of Ultrashort-Pulse Electromagnetic Waves; Nov. 1996

NIFS-463 V. Voitsenya, V. Konovalov, O. Motojima, K. Narihara, M. Becker and B. Schunke,
Evaluations of Different Metals for Manufacturing Mirrors of Thomson Scattering System for the LHD Divertor Plasma; Nov. 1996

NIFS-464 M. Pereyaslavets, M. Sato, T. Shimozuma, Y. Takita, H. Idei, S. Kubo, K. Ohkubo and K. Hayashi,
Development and Simulation of RF Components for High Power Millimeter Wave Gyrotrons; Nov. 1996

NIFS-465 V.S. Voitsenya, S. Masuzaki, O. Motojima, N. Noda and N. Ohyabu,
On the Use of CX Atom Analyzer for Study Characteristics of Ion Component in a LHD Divertor Plasma; Dec. 1996

NIFS-466 H. Miura and S. Kida,
Identification of Tubular Vortices in Complex Flows; Dec. 1996

NIFS-467 Y. Takeiri, Y. Oka, M. Osakabe, K. Tsumori, O. Kaneko, T. Takanashi, E. Asano, T. Kawamoto, R. Akiyama and T. Kuroda,
Suppression of Accelerated Electrons in a High-current Large Negative Ion Source; Dec. 1996

NIFS-468 A. Sagara, Y. Hasegawa, K. Tsuzuki, N. Inoue, H. Suzuki, T. Morisaki, N. Noda, O. Motojima, S. Okamura, K. Matsuoka, R. Akiyama, K. Ida, H. Idei, K. Iwasaki, S. Kubo, T. Minami, S. Morita, K. Narihara, T. Ozaki, K. Sato, C. Takahashi, K. Tanaka, K. Toi and I. Yamada,
Real Time Boronization Experiments in CHS and Scaling for LHD; Dec. 1996

NIFS-469 V.L. Vdovin. T.Watari and A. Fukuyama,
3D Maxwell-Vlasov Boundary Value Problem Solution in Stellarator Geometry in Ion Cyclotron Frequency Range (final report); Dec. 1996

NIFS-470 N. Nakajima, M. Yokoyama, M. Okamoto and J. Nührenberg,
Optimization of M=2 Stellarator; Dec. 1996

NIFS-471 A. Fujisawa, H. Iguchi, S. Lee and Y. Hamada,
Effects of Horizontal Injection Angle Displacements on Energy Measurements with Parallel Plate Energy Analyzer; Dec. 1996

NIFS-472 R. Kanno, N. Nakajima, H. Sugama, M. Okamoto and Y. Ogawa,
Effects of Finite-β and Radial Electric Fields on Neoclassical Transport in the Large Helical Device; Jan. 1997

NIFS-473 S. Murakami, N. Nakajima, U. Gasparino and M. Okamoto,
Simulation Study of Radial Electric Field in CHS and LHD; Jan. 1997

NIFS-474 K. Ohkubo, S. Kubo, H. Idei, M. Sato, T. Shimozuma and Y. Takita,
Coupling of Tilting Gaussian Beam with Hybrid Mode in the Corrugated Waveguide; Jan. 1997

NIFS-475 A. Fujisawa, H. Iguchi, S. Lee and Y. Hamada,
Consideration of Fluctuation in Secondary Beam Intensity of Heavy Ion Beam Prove Measurements; Jan. 1997

NIFS-476 Y. Takeiri, M. Osakabe, Y. Oka, K. Tsumori, O. Kaneko, T. Takanashi, E. Asano, T. Kawamoto, R. Akiyama and T. Kuroda,
Long-pulse Operation of a Cesium-Seeded High-Current Large Negative Ion Source; Jan. 1997

NIFS-477 H. Kuramoto, K. Toi, N. Haraki, K. Sato, J. Xu, A. Ejiri, K. Narihara, T. Seki, S. Ohdachi, K. Adati, R. Akiyama, Y. Hamada, S. Hirokura, K. Kawahata and M. Kojima,
Study of Toroidal Current Penetration during Current Ramp in JIPP T-IIU with Fast Response Zeeman Polarimeter; Jan., 1997

NIFS-478 H. Sugama and W. Horton,
Neoclassical Electron and Ion Transport in Toroidally Rotating Plasmas; Jan. 1997

NIFS-479 V.L. Vdovin and I.V. Kamenskij,
3D Electromagnetic Theory of ICRF Multi Port Multi Loop Antenna; Jan. 1997

NIFS-480 W.X. Wang, M Okamoto, N. Nakajima, S Murakami and N. Ohyabu,
Cooling Effect of Secondary Electrons in the High Temperature Divertor Operation; Feb. 1997

NIFS-481 K. Itoh, S.-I. Itoh, H Soltwisch and H.R. Koslowski,
Generation of Toroidal Current Sheet at Sawtooth Crash; Feb. 1997

NIFS-482 K. Ichiguchi,
Collisionality Dependence of Mercier Stability in LHD Equilibria with Bootstrap Currents; Feb. 1997

NIFS-483 S. Fujiwara and T. Sato,
Molecular Dynamics Simulations of Structural Formation of a Single Polymer Chain: Bond-orientational Order and Conformational Defects; Feb. 1997

NIFS-484 T. Ohkawa,
Reduction of Turbulence by Sheared Toroidal Flow on a Flux Surface; Feb. 1997

NIFS-485 K. Narihara, K. Toi, Y. Hamada, K. Yamauchi, K. Adachi, I. Yamada, K. N. Sato, K. Kawahata, A. Nishizawa, S. Ohdachi. K. Sato, T. Seki, T. Watari, J. Xu, A. Ejiri, S. Hirokura, K. Ida, Y. Kawasumi, M. Kojima, H. Sakakita, T. Ido, K. Kitachi, J. Koog and H. Kuramoto,
Observation of Dusts by Laser Scattering Method in theJIPPT-IIU Tokamak Mar. 1997

NIFS-486 S. Bazdenkov, T. Sato and The Complexity Simulation Group,
Topological Transformations in Isolated Straight Magnetic Flux Tube; Mar. 1997

NIFS-487 M. Okamoto,
Configuration Studies of LHD Plasmas; Mar. 1997

NIFS-488 A. Fujisawa, H. Iguchi, H. Sanuki, K. Itoh, S. Lee, Y. Hamada, S. Kubo, H. Idei, R. Akiyama, K. Tanaka, T. Minami, K. Ida, S. Nishimura, S. Morita, M. Kojima, S. Hidekuma, S.-I. Itoh, C. Takahashi, N. Inoue, H. Suzuki, S. Okamura and K. Matsuoka,
Dynamic Behavior of Potential in the Plasma Core of the CHS Heliotron/Torsatron; Apr. 1997

NIFS-489 T. Ohkawa,
Pfirsch - Schlüter Diffusion with Anisotropic and Nonuniform Superthermal Ion Pressure; Apr. 1997

NIFS-490 S. Ishiguro and The Complexity Simulation Group,
Formation of Wave-front Pattern Accompanied by Current-driven Electrostatic Ion-cyclotron Instabilities; Apr. 1997

NIFS-491 A. Ejiri, K. Shinohara and K. Kawahata,

An Algorithm to Remove Fringe Jumps and its Application to Microwave Reflectometry; Apr. 1997

NIFS-492 K. Ichiguchi, N. Nakajima, M. Okamoto,
Bootstrap Current in the Large Helical Device with Unbalanced Helical Coil Currents; Apr. 1997

NIFS-493 S. Ishiguro, T. Sato. H. Takamaru and The Complexity Simulation Group,
V-shaped dc Potential Structure Caused by Current-driven Electrostatic Ion-cyclotron Instability; May 1997

NIFS-494 K. Nishimura, R. Horiuchi, T. Sato,
Tilt Stabilization by Energetic Ions Crossing Magnetic Separatrix in Field-Reversed Configuration; June 1997

NIFS-495 T. -H. Watanabe and T. Sato,
Magnetohydrodynamic Approach to the Feedback Instability; July 1997

NIFS-496 K. Itoh. T. Ohkawa, S. -I.Itoh, M. Yagi and A. Fukuyama
Suppression of Plasma Turbulence by Asymmetric Superthermal Ions; July 1997

NIFS-497 T. Takahashi, Y. Tomita. H. Momota and Nikita V. Shabrov,
Collisionless Pitch Angle Scattering of Plasma Ions at the Edge Region of an FRC; July 1997

NIFS-498 M. Tanaka, A.Yu Grosberg, V.S. Pande and T. Tanaka,
Molecular Dynamics and Structure Organization in Strongly-Coupled Chain of Charged Particles; July 1997

NIFS-499 S. Goto and S. Kida,
Direct-interaction Approximation and Reynolds-number Reversed Expansion for a Dynamical System; July 1997

NIFS-500 K. Tsuzuki, N. Inoue, A. Sagara, N. Noda, O. Motojima, T. Mochizuki, T. Hino and T. Yamashina,
Dynamic Behavior of Hydrogen Atoms with a Boronized Wall; July 1997

NIFS-501 I. Viniar and S. Sudo,
Multibarrel Repetitive Injector with a Porous Pellet Formation Unit; July 1997

NIFS-502 V. Vdovin, T. Watari and A. Fukuyama,
An Option of ICRF Ion Heating Scenario in Large Helical Device; July 1997

NIFS-503 E. Segre and S. Kida,
Late States of Incompressible 2D Decaying Vorticity Fields; Aug. 1997